ELSEVIER

Volume 182, Number 3, March 2009

JOURNAL OF SOLID STATE CHEMISTRY

www.elsevier.com/locate/jssc

CONTENTS

Abstracted/indexed in BioEngineering Abstracts, Chemical Abstracts, Coal Abstracts, Current Contents/Physics, Chemical, & Earth Sciences, Engineering Index, Research Alert, SCISEARCH, Science Abstracts, and Science Citation Index. Also covered in the abstract and citation database SCOPUS®. Full text available on ScienceDirect®.

Regular Articles

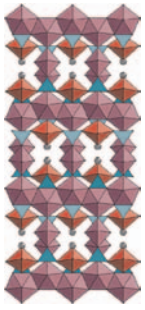

A view of the three-dimensional structure of $Li_3(UO_2)_7(VO_4)_5O$.

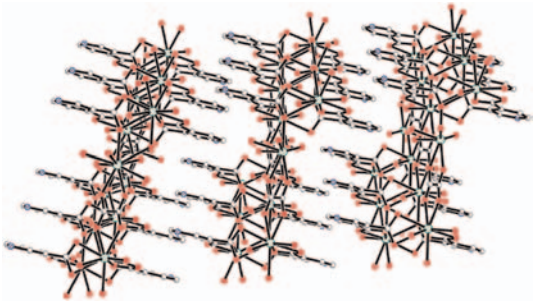

A series of lanthanide-organic frameworks with aromatic pyridinecarboxylate ligands have been successfully synthesized and characterized. Complexes **3** and **5** exhibit strong fluorescent emissions in the visible region at room temperature.

Regular Articles—Continued

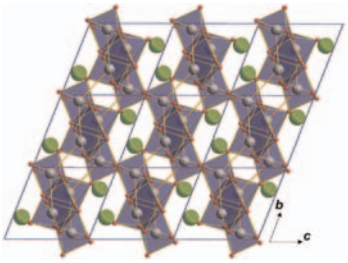

A new modification of KOs_2O_6, the representative of a new structural type (Pearson symbol a$P18$, $a = 5.5668(1)$ Å, $b = 6.4519(2)$ Å, $c = 7.2356(2)$ Å, $\alpha = 65.377(3)^\circ$, $\beta = 70.572(3)^\circ$, $\gamma = 75.613(2)^\circ$ space group $P-1$, no. 2 was synthesized employing high pressure technique. The structure can be described as two OsO_6 octahedral chains relating to each other through inversion and forming big voids with K atoms inside.

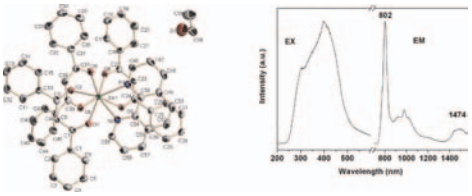

The crystal structure of $Tm(DBM)_3$phen complex (DBM = dibenzoylmethane; phen = 1, 10-phenanthroline). The complex is successfully covalently bonded to MCM-41 ($Tm(DBM)_3$phen-MCM-41). After ligand-mediated excitation, the emission spectrum of $Tm(DBM)_3$phen-MCM-41 shows the bands 802 and 1474 nm. The FWHM of the 1474-nm band for $Tm(DBM)_3$phen-MCM-41 is 110 nm, such a broad spectrum enables a wide gain bandwidth for optical amplification.

Continued

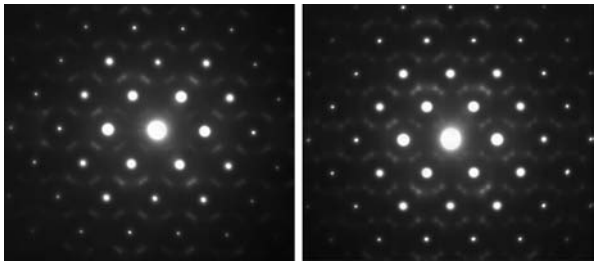

Short-range ordering has been seen in the defect fluorites $Y_2Zr_2O_7$ and $Y_2Hf_2O_7$, where they previously were thought to be entirely disordered. Evidence suggests the correlation length changes with composition, but is not commensurate with unit cell sizes.

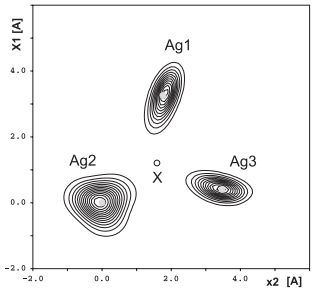

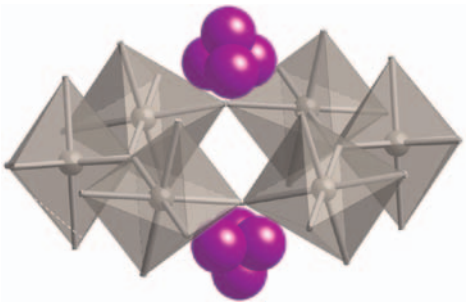

Diagram showing general disorder of K cations in $KAl_{0.33}W_{1.67}O_6$.

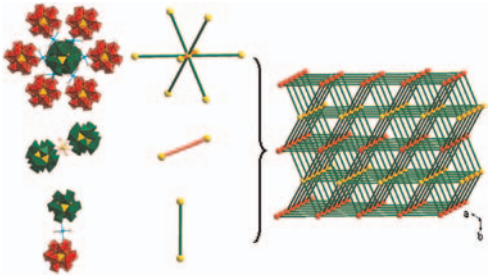

Three extended frameworks based on Silverton-type polyoxometalate have been successfully synthesized. In these compounds, $[Ce^{IV}Mo_{12}O_{42}]^{8-}$ clusters are connected by lanthanide, transition metal and Li^+ to form a $4^{24}56^3$ network.

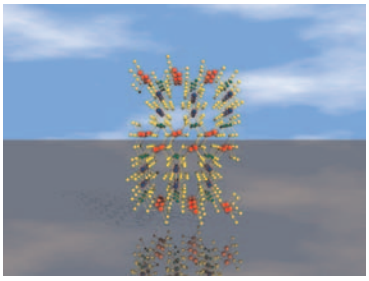

The thiophosphates $Ag_2Nb[P_2S_6][S_2]$ and $KAg_2[PS_4]$ crystallize as three-dimensional networks. A remarkable structural feature of the former compound is a $[Ag_2S_4]$ chain composed of $[AgS_4]$ tetrahedra and $[AgS_3]$ triangles.

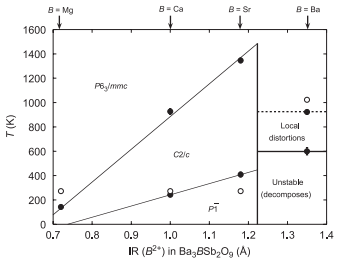

Thermodynamic phase diagram for $Ba_3BSb_2O_9$, B = Mg, Ca, and Sr, as a function of temperature T and effective ionic radius (IR) of the B^{2+} cation.

High-pressure synthesis and crystal structure of the mixed-valent titanium borate $Ti_5B_{12}O_{26}$
Almut Haberer and Hubert Huppertz
Page 484

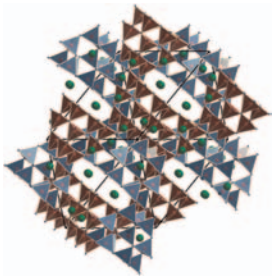

High-pressure/high-temperature synthesis (multianvil technique) led to the first mixed-valent titanium borate $Ti_5B_{12}O_{26}$, which is exclusively built up from corner-sharing BO_4-tetrahedra, showing structural relations to the Zintl phase NaTl.

Comparison of T-piece and concentric mixing systems for continuous flow synthesis of anatase nanoparticles in supercritical isopropanol/water
Lars L. Toft, David F. Aarup, Martin Bremholm, Peter Hald and Bo B. Iversen
Page 491

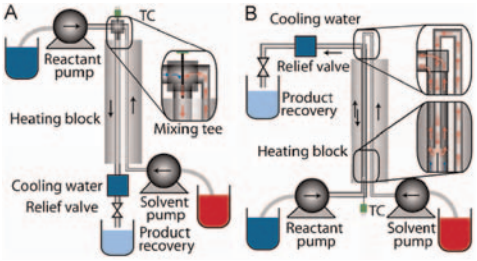

Direct experimental comparison of T-piece and concentric mixing geometries in supercritical continuous flow synthesis of anatase nanoparticles.

Superstructure of a phosphor material $Ba_3MgSi_2O_8$ determined by neutron diffraction data
Cheol-Hee Park, Seung-Tae Hong and Douglas A. Keszler
Page 496

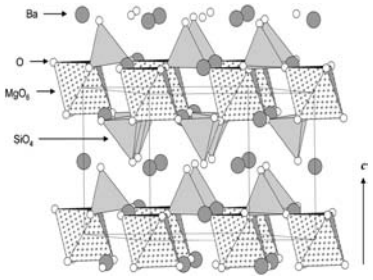

Crystal structure of $Ba_3MgSi_2O_8$ viewed along the *c* direction. Superstructure reflections, observed only in the neutron diffraction data, provided the means to establish the true unit cell and a chemically reasonable structure.

Synthesis, structural characterization and selectively catalytic properties of metal–organic frameworks with nano-sized channels: A modular design strategy
Ling-Guang Qiu, Li-Na Gu, Gang Hu and Li-De Zhang
Page 502

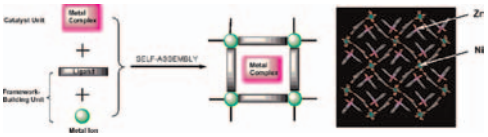

A modular design strategy has been developed to synthesize microporous metal–organic frameworks with potential catalytic activity by self-assembly of the framework-building blocks and the catalyst unit.

Synthesis and crystal structure determination of yttrium ultraphosphate YP_5O_{14}
A. Mbarek, M. Graia, G. Chadeyron, D. Zambon, J. Bouaziz and M. Fourati
Page 509

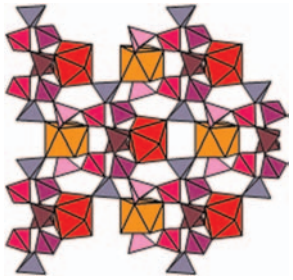

The crystal structure of the monoclinic $C2/c$ polymorph of YP_5O_{14} has been refined from single-crystal X-ray diffraction data. The luminescence properties of the Eu^{3+} ion incorporated in this matrix as local structural probe show that the Eu^{3+} ions are distributed over the two Y^{3+} crystallographic sites of C_2 symmetry of this structure.

Hydrothermal synthesis, characterization, and photocatalytic properties of Zn_2SnO_4
Xianliang Fu, Xuxu Wang, Jinlin Long, Zhengxin Ding, Tingjiang Yan, Guoying Zhang, Zizhong Zhang, Huaxiang Lin and Xianzhi Fu
Page 517

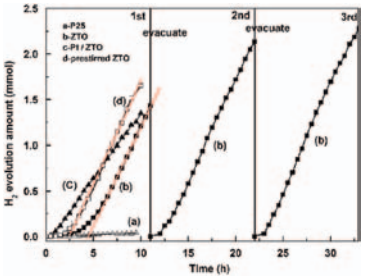

Nanosized Zn_2SnO_4 (ZTO) was successfully synthesized by hydrothermal process. Photocatalytic test showed that the samples exhibited high activity and durability for photodegradation of methyl orange (MO) and photocatalytic production H_2 from ethanol aqueous solution.

Continued

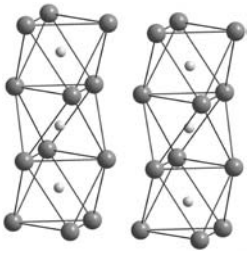

TiI_3 undergoes a first-order phase transition at $T_c = 323\,K$. The dimerization of chains of metal atoms at low temperatures is larger in TiI_3 than in corresponding chlorides and bromides, and thus provides an explanation for the larger inclination of TiI_3 towards dimerization, despite metal–metal bonds being weaker than in chlorides and bromides.

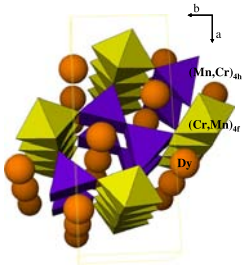

$DyCrMnO_5$ is isostructural with $DyMn_2O_5$, belonging to the *Pbam* space group. The crystal structure contains infinite chains of edge-sharing $Mn^{4+}O_6$ octahedra, interconnected by dimer units of $Cr^{3+}O_5$ square pyramids. The low-temperature neutron powder diffraction (NPD) patterns do not show any magnetic contribution, indicating that a full long-range magnetic ordering is not established down to low temperature, although the Dy^{3+} magnetic moments are susceptible to be polarized by an external magnetic field at the lowest temperature of 5 K.

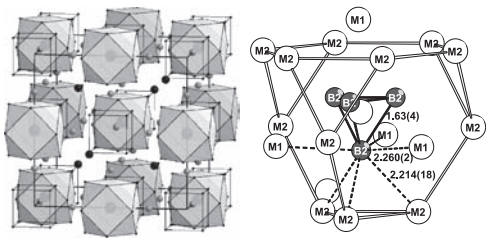

Single crystal investigations on τ-borides Co/M/B with M = Al, Ga, In, Sn, V, Ti, Ir explained the substitution processes. Furthermore the yielded the first binary boride, $Co_{23}B_6$, and a boron-rich $Co_{12.3}Ir_{8.9}B_{10.5}$ containing B_4-tetrahedra.

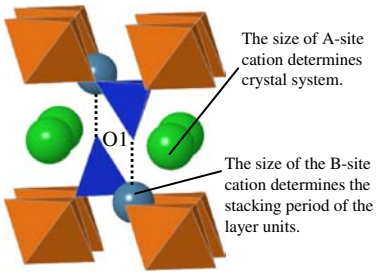

Structure of glaserite-type $M_3MgSi_2O_8$ illustrated with MgO_6 octahedra and SiO_4 tetrahedra.

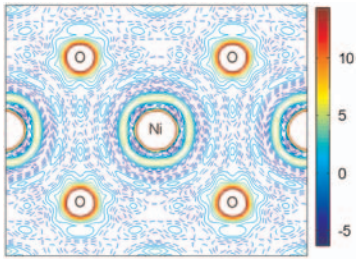

Combining electron and X-ray diffraction data of $LiNiO_2$ in multipole refinement, charge density distribution, topological properties at bond critical points and 3*d* orbital populations of Ni atoms were obtained.

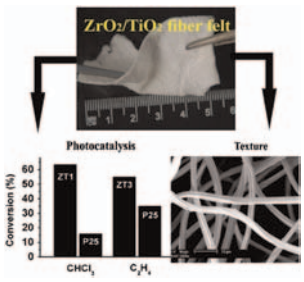

The final ZrO_2/TiO_2 products composed of hollow fibers are in the form of felt on the centimeter scale and possess certain strength and flexibleness. Moreover, they exhibit excellent efficiency and durable activity stability for photodegradation of gaseous ethylene and trichloromethane, reaching about 136% and 387% of the *P*25 activity after 10 h, respectively.

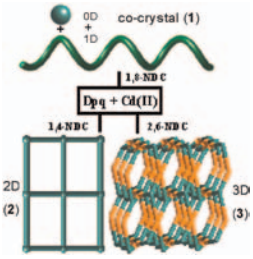

Three novel Cd(II) compounds have been synthesized under hydrothermal conditions exhibiting a systematic variation of architecture by the employment of three structurally related naphthalene-dicarboxylate ligands.

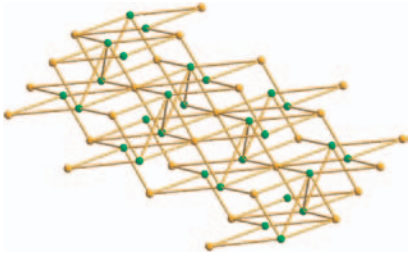

The MOF $[Zn_5(trencba)_2(OH)_2Cl_2 \cdot 4H_2O]$ (H_3trencba = *N*,*N*,*N*′,*N*′,*N*′,*N*′-tris[(4-carboxylate-2-yl)methyl]-tris(2-aminoethyl)amine) reveals a (6,8)-connected bi-nodal three-dimensional porous framework with unprecedented penta-nuclear fragment, which appears to be a good candidate of hybrid inorganic-organic photoactive materials.

Structure of $LiNaMnS_2$. Li and Mn are statistically distributed in edge-shared tetrahedral environments linked into infinite planes. Sodium ions occupy interlayer sites.

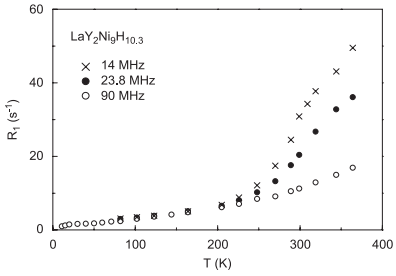

The temperature dependences of the proton spin–lattice relaxation rates R_1 measured at 14, 23.8 and 90 MHz for $LaY_2Ni_9H_{10.3}$. The frequency-dependent increase in R_1 at $T > 250$ K indicates the onset of the motional contribution to the relaxation rates.

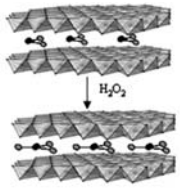

Nitrite intercalated LDHs were prepared by a two –stage process. The interlayer nitrite ions could be quantitatively oxidized to nitrate ions using H_2O_2

Nitrite-intercalated LDHs could be prepared by a two-stage process that involves coprecipitation in the presence of nitrite ions followed by stirring the product with excess of nitrite ions. The interlayer nitrite ions in these LDHs could be quantitatively oxidized to nitrate ions.

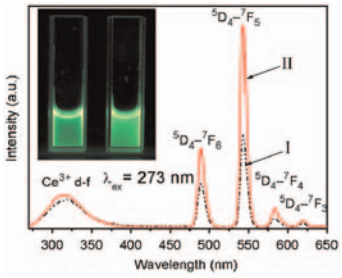

The LaF_3:Ce^{3+}, Tb^{3+} nanocrystals with LaF_3 shells exhibited much stronger emission than the original cores.

Continued

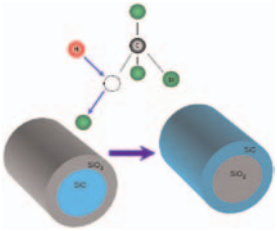

SiC and SiO_2/SiCNWs are shown to be structurally modified through a hydrogen activated replacement route which can even lead to the axial inter-conversion of species. The process could be exploited as a viable route to manipulate a variety of nanostructures and films for doping and etching and structural manipulation.

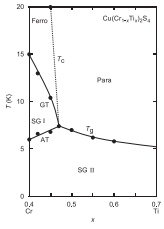

An enlargement of the magnetic phase diagram for $Cu(Cr_{1-x}Ti_x)_2S_4$ at a constant field of 100 Oe over the range of $0.40 \leqslant x \leqslant 0.70$. The curves give a guide to the eye: para, paramagnetic; ferro, ferromagnetic; SGI, spin-glass I (GT-phase), and SGII: spin-glass II (AT-phase). Three characteristic temperatures of T_c, T_{GT}, and T_{AT} merge into 7.40 K at $x = 0.47$ in $H = 100$ Oe. This is a multicritical point.

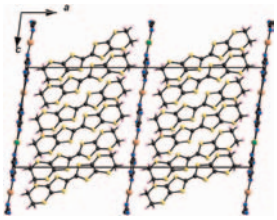

The first polymorph, κ''-$(ET)_2Cu[N(CN)_2]Cl$, of the well known family of isostructural κ-salts $(ET)_2Cu[N(CN)_2]X$ (X = Cl, Br, I) has been prepared and its crystal and electronic structures have been examined. The main structural differences between the monoclinic and orthorhombic polymorphic κ-salts are that in the first the anion sheets are disordered and the ET molecules are less planar. The new polymorph shows metallic type resistivity down to 4.2 K.

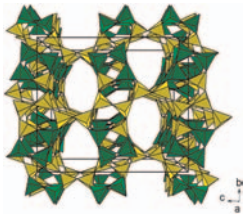

The synthesis and the structure of IM-16 a new germanosilicate with a novel zeolitic topology prepared hydrothermally with the ionic liquid 3-ethyl-1-methyl-3*H*-imidazol-1-ium as the organic structure-directing agent are reported. This new zeolite framework type contains 10-MRs channels and may be described from the *d4r* and *mtw* composite building units.

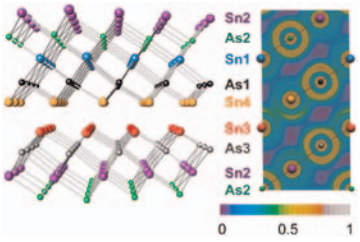

Solvothermally synthesized tin arsenide reveals non-centrosymmetric crystal structure and a complicated chemical bonding pattern including multi-center bonds and lone pairs.

Rapid Communication

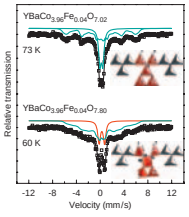

Mössbauer spectroscopy of layered $YBaCo_{3.96}Fe_{0.04}O_{7+\delta}$ ($\delta = 0.02$ and 0.80), with 1% ^{57}Fe isotope substituted for cobalt, revealed no evidence of charge ordering at 4–293 K. The predominant state of iron cations was found trivalent, irrespective of their coordination and oxygen stoichiometry variations determined by thermogravimetric analysis. Decreasing temperature below 75–80 K leads to gradual freezing of the iron magnetic moments in inverse correlation with the content of extra oxygen extending the temperature range where the paramagnetic and frozen states coexist down to 45–50 K.

Author inquiries

For inquiries relating to the submission of articles (including electronic submission where available) please visit this journal's homepage at http://www.elsevier.com/locate/jssc. You can track accepted articles at http://www.elsevier.com/trackarticle and set up e-mail alerts to inform you of when an article's status has changed. Also accessible from here is information on copyright, frequently asked questions and more.
Contact details for questions arising after acceptance of an article, especially those relating to proofs, will be provided by the publisher.

Language services. Authors who require information about language editing and copyediting services pre- and post-submission please visit http://www.elsevier.com/locate/languagepolishing or our customer support site at http://epsupport.elsevier.com. Please note Elsevier neither endorses nor takes responsibility for any products, goods or services offered by outside vendors through our services or in any advertising. For more information please refer to our Terms & Conditions http://www.elsevier.com/termsandconditions

For a full and complete Guide for Authors, please go to: http://www.elsevier.com/locate/jssc

Journal of Solid State Chemistry has no page charges.